Available online at website: https://journal.bcrec.id/index.php/bcrec

Bulletin of Chemical Reaction Engineering & Catalysis, 22 (1) 2027, 134-147

Original Research Article

Catalytic Valorisation of Water Hyacinth Cellulose through Biomimetic Hydrolysis: Integrating Structural Accessibility and Cooperative Acid Catalysis for Renewable Glucose Production

Mey Shelly Rikin[1], Tri Partono Adhi[1]*, Tjokorde Walmiki Samadhi[1], Setyo Yanus Sasongko[2]

[1]Department of Chemical Engineering, Institut Teknologi Bandung, Bandung 40132, Indonesia.
[2]PT. Aimtopindo Nuansa Kimia, Bandung, 40212, Indonesia.

Received: 12th October 2026; Revised: 15th November 2026; Accepted: 16th November 2026
Available online: 20th November 2026; Published regularly: April 2027

Abstract

The catalytic conversion of lignocellulosic biomass into renewable sugars is a key step toward the development of sustainable bio-based chemicals and biorefineries. In this study, cellulose isolated from water hyacinth (*Eichhornia crassipes*), an abundant invasive aquatic biomass, was valorised through biomimetic hydrolysis using piperazinium dihydrogen sulfate (PDS) under mild reaction conditions. Sequential pretreatment was employed to remove non-cellulosic components and improve cellulose accessibility, resulting in a cellulose-rich material with a crystallinity index of 20.1% and fibril diameters of 5–20 nm. Hydrolysis experiments were conducted at cellulose loadings of 1–3 wt%, PDS concentrations of 0.122–0.244 M, and temperatures ranging from 50 to 90 °C. Transition metal ions (Mn, Cu, Fe, Zn, and Ni; 0.006 M) were incorporated as co-catalysts to investigate cooperative Brønsted–Lewis acid activation. The hydrolysis rate increased with increasing temperature, catalyst concentration, and cellulose accessibility, yielding apparent rate constants of 0.0010–0.0346 $mmol.L^{-1}.min^{-1}$. Kinetic analysis revealed fractional reaction orders of 0.80 with respect to cellulose concentration and 0.75 with respect to proton concentration, with activation energies ranging from 65 to 74 $kJ.mol^{-1}$ for the PDS only system. Fe- and Cu-assisted systems exhibited enhanced glucose formation, highlighting the importance of cooperative catalytic interactions during glycosidic bond cleavage. The results demonstrate that effective biomass valorisation depends on the integration of structural accessibility and catalytic activation, providing mechanistic insights for the development of sustainable routes for converting lignocellulosic biomass into renewable sugars and bio-based chemicals.

Copyright © 2027 by Authors, Published by BCREC Publishing Group. This is an open access article under the CC BY-SA License (https://creativecommons.org/licenses/by-sa/4.0).

Keywords: Biomimetic Catalysis; Cellulose Hydrolysis; Renewable Glucose; Transition Metal; Water Hyacinth

How to Cite: Rikin, M. S., Adhi, T. P., Samadhi, T. W., Sasongko, S. Y. (2027). Catalytic Valorisation of Water Hyacinth Cellulose through Biomimetic Hydrolysis: Integrating Structural Accessibility and Cooperative Acid Catalysis for Renewable Glucose Production. *Bulletin of Chemical Reaction Engineering & Catalysis*, 22 (1), 134-147. (DOI: 10.9767/bcrec.20885)

Permalink/DOI: https://doi.org/10.9767/bcrec.20885

1. Introduction

Lignocellulosic biomass has attracted considerable attention as a renewable carbon resource for the sustainable production of fuels, platform chemicals, and bio-based materials due to its abundance, low cost, and wide availability [1–3]. Among various lignocellulosic feedstocks, water hyacinth (*Eichhornia crassipes*) is considered a particularly promising biomass because of its rapid growth rate, high cellulose content, and widespread distribution in tropical and subtropical regions [4–6]. However, uncontrolled proliferation of water hyacinth causes severe environmental problems, including blockage of waterways, oxygen depletion in aquatic ecosystems, and disruption of local biodiversity [7]. Consequently, the utilization of water hyacinth as a renewable feedstock for biomass valorization offers both environmental and economic benefits.

* Corresponding Author.
Email: tpadhi@itb.ac.id (T. P. Adhi)

Cellulose, the major structural component of lignocellulosic biomass, is a linear polysaccharide composed of β-1,4-linked glucose units organized into highly ordered supramolecular structures stabilized by extensive intra- and intermolecular hydrogen bonding [8,9]. The coexistence of crystalline and amorphous regions within cellulose microfibrils contributes to its recalcitrant nature, limiting the accessibility of glycosidic bonds during catalytic conversion processes [10]. As a result, efficient hydrolysis of cellulose remains one of the major challenges in biomass conversion technologies.

Acid-catalyzed hydrolysis is widely employed for the depolymerization of cellulose into glucose and other soluble sugars [11,12]. Nevertheless, conventional mineral acid hydrolysis typically requires high temperatures and harsh reaction conditions, which often lead to low selectivity and the formation of undesirable by-products such as humins and furan derivatives [13,14]. In addition, the apparent hydrolysis kinetics are strongly influenced by structural factors including crystallinity, surface accessibility, and diffusion limitations within the lignocellulosic matrix [15,16]. Therefore, improving cellulose accessibility prior to hydrolysis is essential for enhancing catalytic performance under mild conditions.

Pretreatment plays a crucial role in reducing biomass recalcitrance by removing non-cellulosic components and altering the supramolecular organization of cellulose [17,18]. Structural modifications such as fibril delamination, reduction of crystallinity, disruption of hydrogen-bonding networks, and increased porosity have been reported to improve cellulose reactivity during hydrolysis [19,20]. These changes increase the accessibility of glycosidic bonds and facilitate interactions between catalytic species and cellulose chains.

In recent years, biomimetic catalysis has emerged as a promising strategy for cellulose conversion by reproducing key catalytic functions observed in enzymatic hydrolysis systems [21]. Instead of replicating the structural complexity of enzymes, biomimetic systems are designed to mimic essential catalytic features such as cooperative proton transfer, acid–base interactions, and transition-state stabilization [22]. Catalysts containing Brønsted and Lewis acidic functionalities have demonstrated enhanced catalytic performance for cellulose hydrolysis through synergistic activation of glycosidic bonds [23,24]. Such approaches offer opportunities for achieving controlled depolymerization under milder and more sustainable operating conditions.

In our previous work, piperazinium dihydrogen sulfate (PDS) was introduced as a functionally biomimetic catalyst for cellulose hydrolysis under relatively mild conditions [25]. The catalytic system exhibited cooperative acid–base behavior that facilitated proton-assisted cleavage of β-1,4-glycosidic bonds. However, the relationship between cellulose structural accessibility and hydrolysis kinetics in this biomimetic system has not yet been systematically investigated. In particular, the combined effects of supramolecular structural modification and cooperative Brønsted–Lewis acid interactions on cellulose depolymerization remain insufficiently understood.

Therefore, the present study investigates the structure-dependent kinetics of biomimetic hydrolysis of cellulose derived from water hyacinth. Sequential pretreatment was applied to modify cellulose structure and enhance chain accessibility prior to hydrolysis using piperazinium dihydrogen sulfate in the presence of transition metal co-catalysts. By integrating structural characterization with kinetic analysis, this work aims to elucidate the interplay between biomass structural accessibility, cooperative catalytic activation, and hydrolysis kinetics under mild conditions. The findings are expected to contribute to the development of sustainable catalytic strategies for lignocellulosic biomass valorization and renewable glucose production.

2. Materials and Methods

2.1. Materials

Water hyacinth (*Eichhornia crassipes*) biomass used in this study was collected from a local freshwater body in West Java, Indonesia. The collected biomass represents locally grown water hyacinth plants, as illustrated in Figure 1. Prior to processing, the plants were washed thoroughly with deionized water to remove adhering impurities and air-dried under ambient conditions for 12 hours. Only the stem and leaf portions of the plant were used for cellulose isolation, while roots were excluded to minimize



Figure 1. Local water hyacinth (*Eichhornia crassipes*) collected from a freshwater environment in West Java, Indonesia, used as the biomass source for cellulose isolation.

Copyright © 2027, ISSN 1978-2993

variability associated with sediment contamination. The stem and leaf fractions were mixed in a 1:1 mass ratio before further processing. The chemical composition of the water hyacinth biomass used in this work was determined on a dry-weight basis and is summarized in Table 1. The biomass consists primarily of structural polysaccharides, with hemicellulose and cellulose as the dominant components, accompanied by smaller fractions of lignin, protein, and extractives.

In addition to biomass feedstock, several analytical-grade reagents were used during pretreatment and hydrolysis experiments. Sodium carbonate (Na_2CO_3), sodium dodecyl sulfate (SLS), 1M hydrochloric acid (HCl), ethanol, sodium chlorite ($NaClO_2$), glacial acetic acid, and sodium hydroxide (NaOH) were employed during the sequential pretreatment steps for extractive removal, deproteinization, delignification, and hemicellulose extraction. Piperazine and sulfuric acid (H_2SO_4) were used to prepare the biomimetic catalyst piperazinium dihydrogen sulfate (PDS). For the investigation of cooperative catalytic effects, several transition metal salts were introduced as co-catalysts, including manganese sulfate ($MnSO_4 \cdot H_2O$), copper sulfate ($CuSO_4 \cdot 5H_2O$), iron sulfate ($FeSO_4 \cdot 7H_2O$), zinc sulfate ($ZnSO_4 \cdot 7H_2O$), and nickel sulfate ($NiSO_4 \cdot 6H_2O$). Transition metal ions can provide Lewis acidic sites capable of interacting with hydroxyl groups in cellulose and promoting glycosidic bond polarization during hydrolysis reactions. All chemicals were of analytical grade and used as received without further purification. Deionized water was used throughout all experimental procedures.

The compositional analysis further demonstrated that cellulose and hemicellulose together accounted for approximately 71 wt% of the dry biomass, confirming that water hyacinth represents a promising lignocellulosic feedstock for biomass valorization and renewable glucose production.

2.2. Preparation of Pretreated Cellulose

Cellulose-rich material was isolated from water hyacinth through sequential pretreatment designed to remove non-cellulosic components and improve cellulose accessibility. Although the procedure involves conventional biomass pretreatment steps, in the present work it is primarily intended to generate a cellulose fraction with altered structural accessibility suitable for kinetic investigation. The pretreatment protocol was adapted from our previously reported procedure [25], with emphasis placed on disrupting hydrogen-bonded crystalline domains and promoting fibril opening while preserving the cellulose backbone. The sequential treatments consisted of deproteinization, extractive removal, delignification, and hemicellulose extraction.

Table 1. Chemical composition of the water hyacinth biomass employed in this work, expressed on a dry-weight basis.

Component	Content [%]
Extractive	7.80 ± 2.39
Protein	8.40 ± 1.07
Lignin	12.70 ± 2.32
Hemicellulose	35.27 ± 3.16
Cellulose	35.83 ± 3.39

Initially, deproteinization was performed using a mild alkaline–surfactant system containing sodium carbonate (Na_2CO_3) and sodium dodecyl sulfate (SLS) at pH of 8. Aquatic biomass contains significant protein fractions that can competitively bind to catalytic sites and sterically hinder cellulose accessibility. This method was selected because the mild alkaline buffer disrupts electrostatic protein–matrix interactions while the anionic surfactant solubilizes hydrophobic proteins, achieving high protein removal efficiency while preserving the structural integrity of the carbohydrate backbone [28,29,30].

The resulting solid was subsequently subjected to ethanol extraction to eliminate low-molecular-weight extractives such as pigments, waxes, and soluble organic compounds. Delignification was then carried out using an acidified sodium chlorite ($NaClO_2$–acetic acid) solution. This method was specifically selected because the in situ generated chlorine dioxide selectively oxidizes and solubilizes aromatic lignin structures while minimizing carbohydrate degradation and preserving the cellulose degree of polymerization [31]. Following delignification, hemicellulose extraction was performed using a 0.5 N dilute sodium hydroxide solution ($50\,^{\circ}C$, $3.5\,h$, solid-to-liquid ratio of $1:150\ g.mL^{-1}$) to selectively cleave ester linkages and dissolve hemicellulose, yielding a purified cellulose-rich fraction.

After each pretreatment stage, the solid residue was washed repeatedly with deionized water until a neutral pH was achieved and dried to a constant weight. Based on the compositional mass balance (Table 1), the sequential removal of non-cellulosic fractions corresponds to stage-wise solid mass reductions of approximately 8.4% after deproteinization, 7.8% after extractive removal, 12.7% after delignification, and 35.3% after hemicellulose extraction (representing a cumulative solid mass loss of ~64.2%), yielding a final purified cellulose recovery of approximately 35.8% relative to the initial dry biomass. The resulting cellulose fraction was used as the substrate for structural characterization and biomimetic hydrolysis experiments.

Copyright © 2027, ISSN 1978-2993

2.3. Structural Characterizations

The structural evolution of cellulose during pretreatment was analyzed using X-ray diffraction (XRD), Fourier-transform infrared spectroscopy (FTIR), scanning electron microscopy (SEM), transmission electron microscopy (TEM), and thermogravimetric analysis (TGA). X-ray diffraction (XRD) was used to assess changes in crystalline structure and supramolecular order of cellulose before and after pretreatment. X-ray diffraction (XRD) analysis was performed using a Bruker D2 Phaser diffractometer equipped with Cu Kα radiation (λ = 1.5406 Å), operated at 30 kV and 10 mA. Diffraction patterns were recorded over a 2θ range of 5–100° with a step size of 0.02° and a scanning speed of 2 °.min^{-1}. Cellulose samples were finely ground to obtain a homogeneous powder and placed on a flat sample holder with a smooth surface to minimize preferred orientation effects. The crystallinity index (CI) was calculated using the Segal method [26]. The Segal method (or empirical crystallinity index, CI) is a rapid X-ray diffraction (XRD) technique used to estimate cellulose crystallinity by comparing the intensity of the crystalline 002 peak (I_{002}) and the amorphous scatter (I_{am}). It is defined as:

$$CI = \frac{I_{002} - I_{am}}{I_{002}} x100 \quad (1)$$

where I_{002} is measured around 2θ = 22.5^{o} and I_{am} at 2θ = 18^{o} for cellulose.

Fourier-transform infrared spectroscopy (FTIR) was employed to examine modifications in hydrogen bonding and chemical environments within the cellulose matrix. FTIR spectra were obtained using a Bruker FTIR spectrometer equipped with an attenuated total reflectance (ATR) accessory. Solid samples were directly placed onto the ATR crystal and pressed gently to ensure proper contact without additional preparation. Morphological evolution and fibril accessibility were analyzed using scanning electron microscopy (SEM) and transmission electron microscopy (TEM), from which representative fibril diameters were estimated. SEM images were obtained using a Hitachi SU3500 scanning electron microscope operated at an accelerating voltage of 10–15 kV. Samples were mounted on aluminum stubs using conductive carbon tape and sputter-coated with a thin layer of gold to enhance electrical conductivity and reduce charging effects during imaging. TEM analysis was performed using a Hitachi HT7700 transmission electron microscope operating at an accelerating voltage of 100 kV. Cellulose samples were dispersed in ethanol and ultrasonicated for 10–15 minutes to achieve uniform dispersion. A drop of the suspension was deposited onto a carbon-coated copper grid and allowed to dry at room temperature prior to imaging. Thermogravimetric analysis (TGA) was conducted to evaluate changes in thermal stability associated with structural modification, providing complementary insight into differences in polymer ordering. Thermal analysis was carried out using a Hitachi STA7300 simultaneous TG/DTA instrument. Approximately 2–3 mg of sample was placed in an alumina crucible and heated from room temperature to 300 °C at a heating rate of 10 °C.min^{-1}.

2.4. Biomimetic Hydrolysis Experiments

Biomimetic hydrolysis experiments were conducted in batch mode under atmospheric pressure. All hydrolysis experiments were conducted as single-batch kinetic runs using fresh pretreated cellulose and freshly prepared catalytic solutions; multi-cycle reusability tests were not performed in this kinetic study, eliminating any inter-run material loss. Pretreated cellulose (1 or 3 wt%) was dispersed in aqueous PDS solutions at concentrations of 0.122 M or 0.244 M, selected based on our prior work [25] to ensure effective biomimetic proton transfer while avoiding secondary sugar degradation. Selected transition metals (Mn, Cu, Fe, Zn, or Ni) were introduced at a fixed low concentration of 0.006 M (a 1: 20 molar ratio relative to 0.122 M PDS) so that the divalent cations function strictly as catalytic Lewis acid promoters without altering the bulk ionic strength or pH of the aqueous phase.

The reaction mixture was heated to the desired temperature (50–90 °C) under constant stirring to minimize external mass-transfer limitations. Aliquots were withdrawn under continuous, uniform stirring to ensure representative sampling of the suspension, thereby maintaining a constant solid-to-liquid ratio within the reactor without altering the bulk cellulose concentration (wt%) during the kinetic run. Glucose concentration in the liquid phase was quantified using established analytical methods. Glucose yield (YG) was evaluated based on the concentration of glucose present in the hydrolysate. The glucose content was quantified using the 3,5-dinitrosalicylic acid (DNS) colorimetric method, with absorbance measured at 540 nm using a UV–Vis spectrophotometer. The glucose concentration (CG, g.L^{-1}) was determined from a calibration curve generated using standard glucose solutions. The glucose yield was subsequently calculated using the following expression:

$$YG\ (\%) = \frac{CG\ x\ V}{W0\ x\ f} x100 \quad (2)$$

Copyright © 2027, ISSN 1978-2993

where W_0 is the initial dry weight of cellulose (g), V is the total volume of the hydrolysate (L), and f is the stoichiometric conversion factor of cellulose to glucose (1.11).

2.5. Kinetic Analysis

Hydrolysis rates were determined from the temporal evolution of glucose concentration in the liquid phase. Under the investigated conditions, glucose concentration increased approximately linearly with reaction time, permitting the apparent rate of glucose formation (r, mmol L^{-1} min^{-1}) to be estimated from the slope of the concentration–time profile. The apparent kinetic behaviour was described using a power-law rate expression of the form:

$$r = k.C_{\text{cell}}^{m}.C_{H^+}^{n} = k_{app} \quad (3)$$

where $k_{\text{app}} = k \cdot C_{\text{cell}}^{m} \cdot C_{H^+}^{n}$ represents the composite apparent rate constant ($\text{mmol.L}^{-1}.\text{min}^{-1}$) evaluated at fixed C_{cell} and C_{H^+}, while k denotes the intrinsic rate constant. The values reported in Tables 3, 5, and 7 represent k_{app} at the specific experimental conditions used in each experiment, from which the Arrhenius parameters are derived. C_{cell} represents the initial cellulose loading (wt%), and C_{H^+} denotes the nominal molar concentration of the PDS catalyst (0.122 M or 0.244 M), which serves as a direct measure of the total stoichiometric proton-donating sites available in the biomimetic proton-relay system. Because PDS transfers protons cooperatively via both piperazinium cations and bisulfate anions, defining C_{H^+} based on nominal catalyst molarity avoids the limitations of bulk pH measurements, while partial dissociation and surface-saturation effects are captured within the apparent reaction order n.

The apparent composite rate constant k_{app} at each temperature was determined from the slope of the glucose concentration–time profile under each specific set of experimental conditions. The apparent reaction orders m and n were determined using a paired-experiment logarithmic comparison approach: m was obtained from experiments at 1 wt% and 3 wt% cellulose loading at fixed PDS concentration (0.122 M), and n was obtained from experiments at 0.122 M and 0.244 M PDS at fixed cellulose loading (1 wt%). At each temperature, the reaction order was calculated as: $m = \ln(k_{\text{app},3\%} / k_{\text{app},1\%}) / \ln(3/1)$, and $n = \ln(k_{\text{app},0.244} / k_{\text{app},0.122}) / \ln(0.244/0.122)$. The mean values across all temperatures are reported as the apparent reaction orders. The temperature dependence of the apparent rate constants was analyzed using the Arrhenius equation:

$$k = A\exp\left(-\frac{E_a}{RT}\right) \quad (4)$$

where A is the pre-exponential factor, E_a is the activation energy, R is the universal gas constant, and T is the absolute temperature.

Activation energies (E_a) and pre-exponential factors (A) were determined from linear regression of ln k versus $1/T$. All kinetic parameters reported in this study are apparent kinetic parameters representing the combined effects of intrinsic bond cleavage, structural accessibility of cellulose, diffusion limitations, and cooperative catalytic interactions within the heterogeneous hydrolysis system.

3. Results and Discussion

This section presents the structural evolution of water hyacinth cellulose during sequential pretreatment and its influence on biomimetic hydrolysis performance under mild conditions, integrating structural characterization with kinetic analysis to elucidate the relationship between biomass accessibility, catalytic activation, and glucose formation. The sequential pretreatment plays a crucial role in restructuring the supramolecular organization of cellulose by progressively removing non-cellulosic components and disrupting the lignocellulosic matrix. This structural evolution is reflected in the crystallographic, spectroscopic, morphological, and thermal characteristics of the resulting cellulose fraction, which in turn govern its reactivity during catalytic depolymerization.

3.1. Pretreatment Induced Structural Modification and Biomass Accessibility

The sequential pretreatment applied to water hyacinth (*Eichhornia crassipes*) biomass plays a fundamental role in restructuring the supramolecular organization of cellulose by progressively removing non-cellulosic components and disrupting the recalcitrant lignocellulosic matrix. The initial chemical composition analysis on a dry-weight basis (Table 1) revealed that cellulose and hemicellulose together accounted for approximately 71 wt% of the raw biomass, validating its high potential as a renewable resource for bio-based chemicals. However, the native cell wall network acts as a major mass-transfer barrier, necessitating targeted structural modification before catalytic conversion.

The successful progression of each pretreatment stage was qualitatively and quantitatively confirmed by visual transformations, mineral removal, and changes in the macromolecular ordering of the polymer matrix. As shown in Figure 2, the raw water hyacinth initially exhibited a dark greenish-brown color due to embedded chlorophyll, matrix proteins, and lignin-derived chromophoric compounds. Following sequential deproteinization and extractive removal, the

Copyright © 2027, ISSN 1978-2993

material became noticeably lighter, reflecting the successful extraction of soluble organic compounds and low-molecular-weight organic structures. A stark transition to a yellowish-whitish appearance occurred after the acidified sodium chlorite delignification stage, which is directly attributed to the heterolytic cleavage of the conjugated aromatic π-electron systems within lignin that are responsible for light absorption. After the final hemicellulose extraction stage using dilute sodium hydroxide, the purified substrate appeared as a pale whitish fibrous matrix, indicating a high-purity cellulose-rich material with extensive matrix exposure.

This progressive purification is directly validated by the non-monotonic evolution of the empirical Crystallinity Index (CI) determined through X-ray diffraction (XRD) analysis (Table 2 and Figure 3). The native water hyacinth exhibited a baseline CI of 22.4%. A significant contraction in crystallinity was observed immediately after deproteinization (13.9%), extractive removal (11.9%), and delignification (11.4%). This initial downward trend indicates that the disruption of the cell wall matrix simultaneously fragments the highly ordered intra- and intermolecular hydrogen-bonding networks that stabilize native cellulose microfibrils, successfully expanding the exposed amorphous domains.

Interestingly, after the final hemicellulose extraction step, the empirical CI rose back to 20.1% in the isolated cellulose fraction. From a polymer physics perspective, this non-monotonic behavior does not imply a true recrystallization process; instead, it is a structural artifact driven by the highly selective chemical dissolution of the remaining amorphous matrix components (lignin and hemicellulose), leading to a significant relative enrichment of the crystalline cellulose domains within the final sample. This balanced duality between structural opening and crystalline domain enrichment is critical because the reduction of structural constraints directly dictates the geometric accessibility of the β-1,4-glycosidic linkages to the bulky molecular species in the heterogeneous catalyst phase.

The modification of these intra- and intermolecular hydrogen-bonded networks was further evaluated via Fourier-transform infrared spectroscopy (FTIR) (Figure 4). The broad,

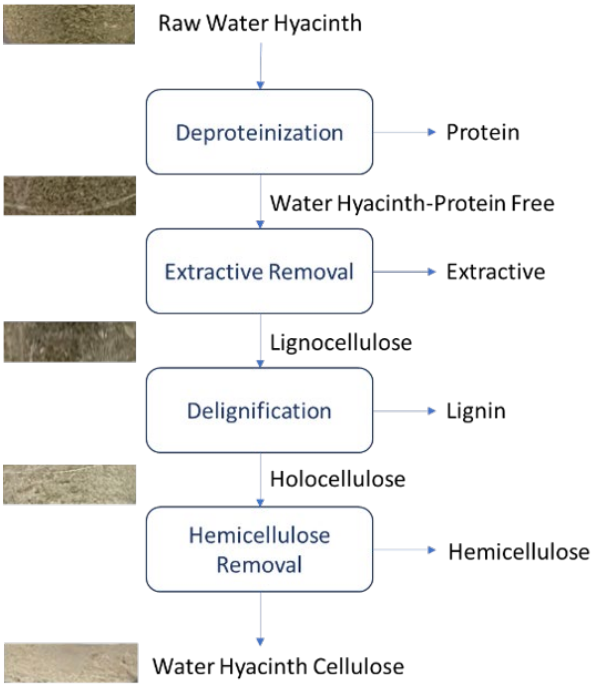


Figure 2. Color change of water hyacinth before and after pretreatment.

Table 2. Crystallinity index before and after pretreatment.

Sample	Crystallinity Index [%]
Water Hyacinth	22.4
Deproteinization	13.9
Extractive Removal	11.9
Delignification	11.4
Water Hyacinth Cellulose	20.1

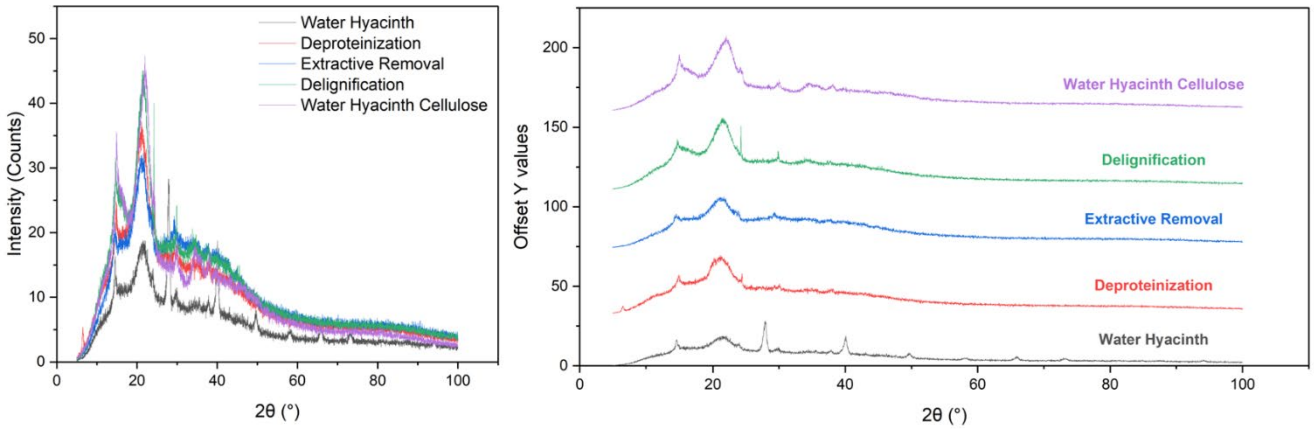


Figure 3. XRD patterns of raw water hyacinth, the pretreatment stages, and the water hyacinth cellulose.

Copyright © 2027, ISSN 1978-2993

dominant absorption band in the region of 3200–3500 cm^{-1}, corresponding to the O–H stretching vibrations, exhibited distinct widening and variations in relative intensity following chemical processing. These spectral shifts indicate a noticeable alteration in the local hydrogen-bonding chemical environments, leading to decreased packing density and enhanced chain mobility within the polymer network. Concurrently, the sharp reduction and eventual disappearance of the characteristic aromatic C=C stretching bands (~1500–1600 cm^{-1}) and carbonyl C=O stretching vibrations (~ 1700 cm^{-1}) confirmed the efficient, stepwise removal of the surrounding lignin and hemicellulose constraints without introducing new chemical functional groups onto the carbohydrate backbone.

These structural modifications are visually validated by the SEM and TEM micrographs (Figures 5 and 6). Scanning electron microscopy of the native biomass showed dense, highly aggregated, and compact fiber bundles tightly cemented within a smooth lignocellulosic matrix. Following sequential processing, this dense architecture underwent deep fragmentation and delamination, revealing severe surface roughness, porous macrostructures, and extensive individual fibril separation caused by the collapse of the cross-linked lignin-carbohydrate complexes. Transmission electron microscopy further revealed that the isolated cellulose fraction consists of nanofibrillar structures with distinct diameters ranging from 5 to 20 nm. This deep nanoscale fibrillation represents a major expansion of the available structural surface area, successfully presenting exposed glycosidic linkages that were previously buried within the core of the native cell wall matrix.

The thermal degradation behavior evaluated via simultaneous DTA, TG, and DTG analysis (Figures 7, 8, and 9) provides complementary evidence of this purification. The mass loss profiles across all samples revealed three primary phases: an initial low-temperature endothermic weight loss (30–120 °C) corresponding to the removal of weakly bound physically adsorbed water, followed by a primary rapid thermal volatilization stage (200–350 °C) driven by the depolymerization and random cleavage of the β -1,4-glycosidic bonds, and a gradual high-temperature char decomposition phase leaving approximately 60% residual mass under inert gas flow. Because cellulose possesses a highly stable semicrystalline matrix stabilized by hydrogen bonding, it undergoes rapid pyrolytic decomposition before reaching a classical thermodynamic melting point (T_m) or glass transition (T_g). Following pretreatment, the primary DTG peak became substantially sharper and more symmetrical, reflecting the successful elimination of low-temperature volatile extractives, proteins, and hemicelluloses, thereby resulting in a highly uniform cellulose material with single-component thermal decomposition behavior.

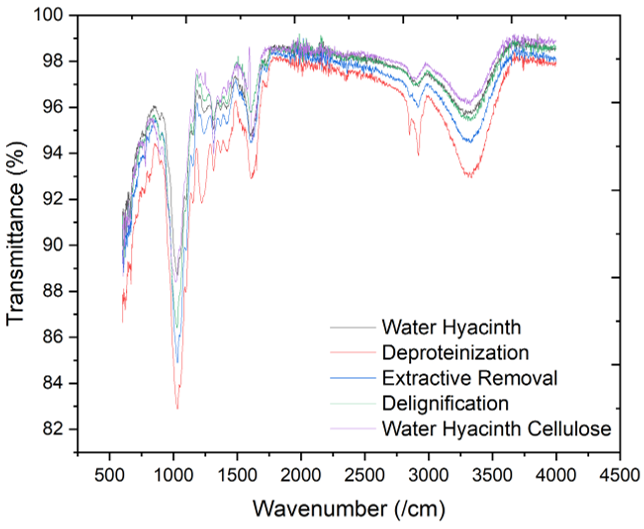


Figure 4. FTIR spectra of raw water hyacinth, the pretreatment stages, and the final water hyacinth

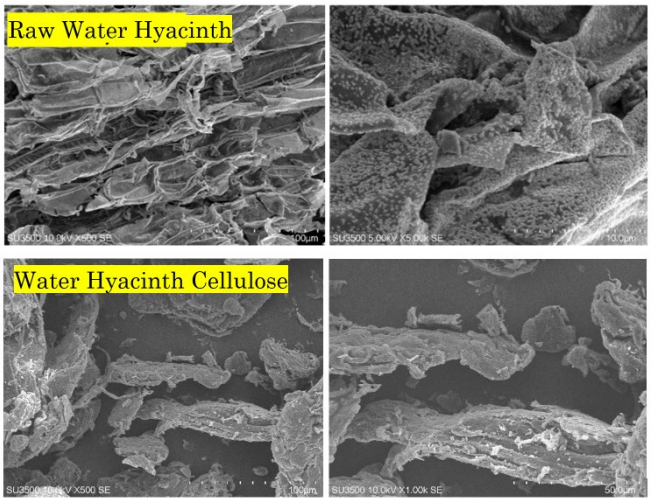


Figure 5. SEM micrographs showing the progressive structural modification of water hyacinth fibers during pretreatment: raw water hyacinth and cellulose.

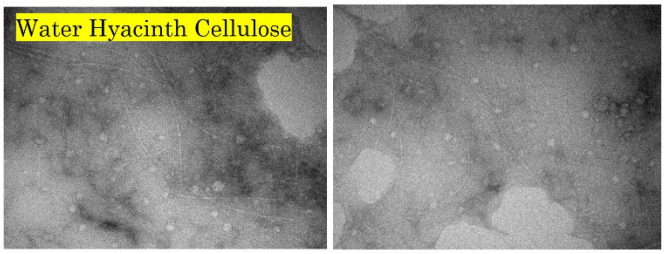


Figure 6. TEM micrographs showing the cellulose fraction of water hyacinth after the pretreatment process.

Copyright © 2027, ISSN 1978-2993

3.2. Biomimetic Catalytic Hydrolysis

The depolymerization of the pretreated water hyacinth cellulose was evaluated using Piperazinium Dihydrogen Sulfate (PDS) as a functionally biomimetic acid catalyst. Across all operating conditions, the liquid-phase glucose yield (Y_G) exhibited a progressive, linear increase throughout the 420-min (7-h) reaction window. This extended linear behavior arises because total cellulose conversion remained within the low-conversion regime ($< 19\%$ in Figure 10) under mild temperatures (50–90 °C), where consecutive glucose dehydration to humins or furans is suppressed. Moreover, as surface glycosidic bonds are cleaved, progressive fibril swelling exposes underlying chains, maintaining an effectively constant surface concentration of accessible reactive sites and resulting in pseudo-zero-order temporal linearity.

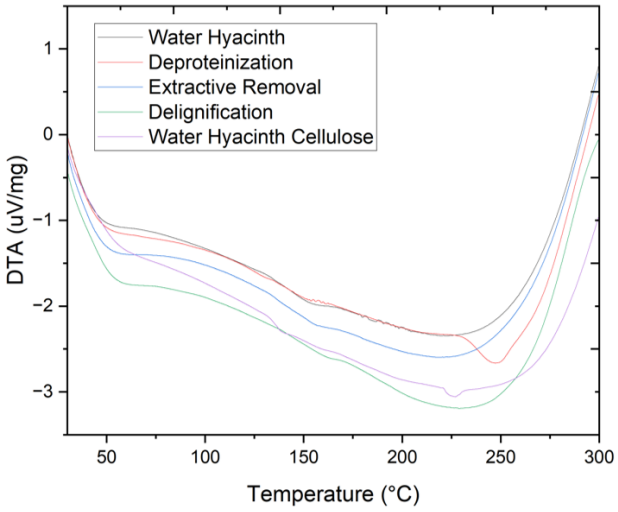


Figure 7. Differential thermal analysis (DTA) thermogram of pretreated cellulose derived from water hyacinth biomass.

3.2.1. Influence of reaction temperature and PDS catalyst concentration

The operational effects of reaction temperature (50–90 °C) and Brønsted acid site availability were simultaneously evaluated at fixed substrate loadings by shifting the PDS catalyst concentration from 0.122 M to 0.244 M (Figure 10). Elevated reaction temperatures dramatically accelerated the rate of glucose accumulation under all scenarios, confirming that the cleavage of the rugged β-1,4-glycosidic bonds is a highly temperature-sensitive, thermally activated pathway. As summarized in Table 3, the extracted composite apparent rate constants (k_{app}) grew systematically from an initial value of 0.0010 $\text{mmol.L}^{-1}.\text{min}^{-1}$ at 50 °C to 0.0213 $\text{mmol.L}^{-1}.\text{min}^{-1}$ at 90 °C. Linear regression analysis via the Arrhenius equation generated strong linear correlations ($R^2 \geq 0.94$), revealing apparent activation energies (E_a) of 69.21 kJ/mol at 0.122 M PDS and 65.51 kJ/mol at 0.244 M PDS (Table 4).

3.2.2. Influence of heterogeneous cellulose loading

To map the kinetics regarding substrate availability, the initial cellulose loading was expanded from 1 wt% to 3 wt% at a fixed PDS loading of 0.122 M (Figure 11). The apparent rate constants rose from $0.0010 - 0.0132$ $\text{mmol.L}^{-1}.\text{min}^{-1}$ for the 1 wt% system to $0.0022 - 0.0346$ $\text{mmol.L}^{-1}.\text{min}^{-1}$ for the 3 wt% system (Table 5). Constructing the corresponding Arrhenius plots yielded an apparent activation energy of 74.02 kJ/mol for the dense 3 wt%

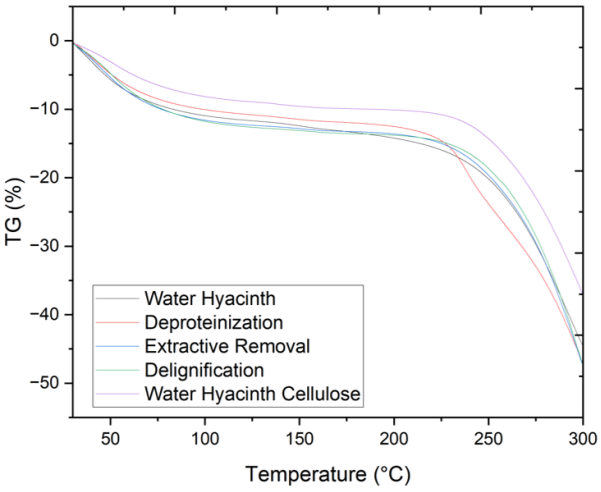


Figure 8. Thermogravimetric (TG) curve of pretreated cellulose obtained from water hyacinth biomass.

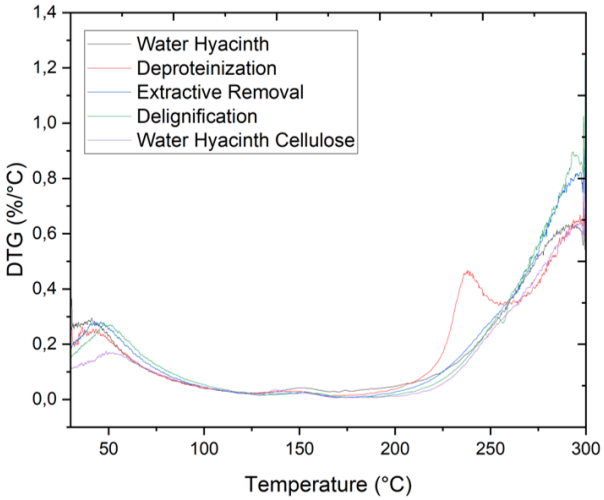


Figure 9. Derivative thermogravimetric (DTG) curve of pretreated cellulose obtained from water hyacinth biomass.

Copyright © 2027, ISSN 1978-2993

suspension compared to 69.21 kJ/mol for the dilute 1 wt% control (Table 6). The slight upward adjustment in the apparent activation energy barrier at higher solid content highlights the introduction of mild external mass-transfer restrictions and local diffusion limitations within the thick, viscous heterogeneous reaction phase.

3.2.3. Kinetic analysis

By executing a paired-experiment logarithmic comparison framework across these variables, the partial empirical reaction orders regarding cellulose concentration (m) and effective proton availability (n) were isolated at each temperature (Tables 7 and 8). The mean values were robustly evaluated as $m = 0.80 \pm 0.068$ and $n = 0.75 \pm 0.093$, culminating in the final power-law rate expression:

$$r = A \exp\left(-\frac{E_a}{RT}\right) C_{\text{cell}}^{0.80} C_{H^+}^{0.75} \quad (5)$$

The fractional order regarding the carbohydrate substrate ($m = 0.80 < 1$) serves as direct kinetic evidence of a highly heterogeneous polymer reaction. Rather than depending on the total concentration of added solid cellulose, the true rate of depolymerization is restricted by the absolute geometric fraction of accessible glycosidic bonds situated along the open surfaces of the nanoscale microfibrils. The mild, systematic expansion of m from 0.72 at 50 °C to 0.88 at 90 °C (Table 8) is physically consistent

Table 4. Activation energy (E_a) and pre-exponential factor (A) for cellulose hydrolysis catalyzed by PDS at 0.122 M and 0.244 M.

[PDS]	E_a [kJ/mol]	A
0.122 M	69.21	1.33×10^8
0.244 M	65.51	6.09×10^7

Table 6. Activation energy (E_a) and pre-exponential factor (A) obtained from Arrhenius analysis of cellulose hydrolysis at 1 wt% and 3 wt%.

[Cellulose]	E_a [kJ/mol]	A
1%	69.21	1.33×10^8
3%	74.02	1.72×10^9

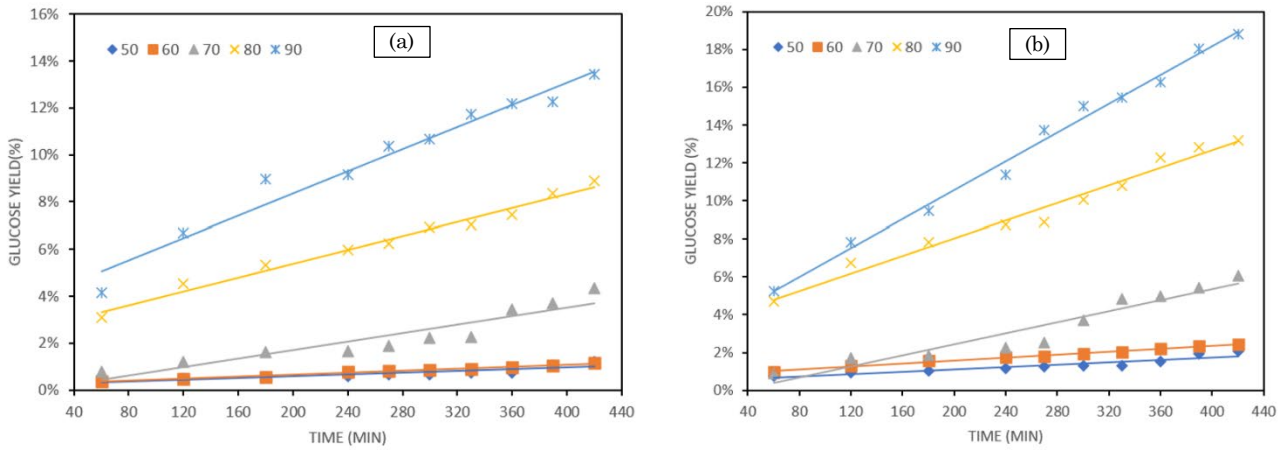


Figure 10. Glucose formation profiles as a function of reaction time at 50–90 °C using PDS catalysts at concentrations of (a) 0.122 M and (b) 0.244 M.

Table 3. Apparent rate constants (k, mmol.L^{-1}.min^{-1}) for cellulose hydrolysis at various reaction temperatures using PDS at 0.122 M and 0.244 M.

PDS [M] / T [°C]	50	60	70	80	90
0.122	0.0010	0.0012	0.0051	0.0083	0.0132
0.244	0.0018	0.0022	0.0082	0.0130	0.0213

Table 5. Apparent rate constants (k, mmol.L^{-1}.min^{-1}) for cellulose hydrolysis at different reaction temperatures using cellulose loadings of 1 wt% and 3 wt%.

Cellulose [%]/ T [°C]	50	60	70	80	90
1%	0.0010	0.0012	0.0051	0.0083	0.0132
3%	0.0022	0.0027	0.0117	0.0216	0.0346

Copyright © 2027, ISSN 1978-2993

with the thermal swelling of the isolated nanofibrils at elevated temperatures, which lowers the hydrogen-bonding network density and expands the exposed reactive surface area.

Concurrently, the sub-linear reaction order regarding proton availability ($n = 0.75 < 1$) indicates a non-ideal catalytic pathway governed by adsorption equilibria and site saturation. This behavior is directly driven by the functional biomimetic proton-relay mechanism of the PDS catalyst, which closely mimics the cooperative acid-base environments observed within enzymatic glycosidase active pockets (Figure 12).

As illustrated in Figure 12, the protonated piperazinium organic cation (NH^+) acts as a flexible Brønsted acid proton donor that targets the glycosidic oxygen atom, inducing polarization and weakening the tough C–O linkage to generate an oxonium-like transition state. Simultaneously, the adjacent hydrogen sulfate anion (HSO_4^-) acts cooperatively as a proton acceptor and a hydrogen-bonding anchor site, stabilizing the localized charge distribution and accelerating heterolytic bond scission.

Because this biomimetic catalyst operates via a tight, coordinated relay network, expanding the nominal proton loading eventually leads to local saturation of the operational relay pathways. As a result, the effective concentration of active protons scales non-linearly, yielding a sub-linear dependency. Crucially, as summarized in the comprehensive literature comparison (Table 9), the apparent activation energies isolated for the PDS system (65–74 kJ/mol) are dramatically lower than the severe energetic barriers required by conventional dilute sulfuric

Table 7. Determination of apparent reaction order n.

T [°C]	$k_{0.122}$	$k_{0.244}$	k ratio	n
50	1.000×10^{-3}	1.800×10^{-3}	1.800	0.848
60	1.200×10^{-3}	2.200×10^{-3}	1.833	0.875
70	5.100×10^{-3}	8.200×10^{-3}	1.608	0.685
80	8.300×10^{-3}	1.300×10^{-2}	1.566	0.647
90	1.320×10^{-2}	2.130×10^{-2}	1.614	0.690
		Mean		0.749 ± 0.093

Table 8. Determination of apparent reaction order m.

T [°C]	$k_{1\%}$	$k_{3\%}$	k ratio	m
50	1.000×10^{-3}	2.200×10^{-3}	2.200	0.718
60	1.200×10^{-3}	2.700×10^{-3}	2.250	0.738
70	5.100×10^{-3}	1.170×10^{-2}	2.294	0.756
80	8.300×10^{-3}	2.160×10^{-2}	2.602	0.871
90	1.320×10^{-2}	3.460×10^{-2}	2.621	0.877
		Mean		0.792 ± 0.068

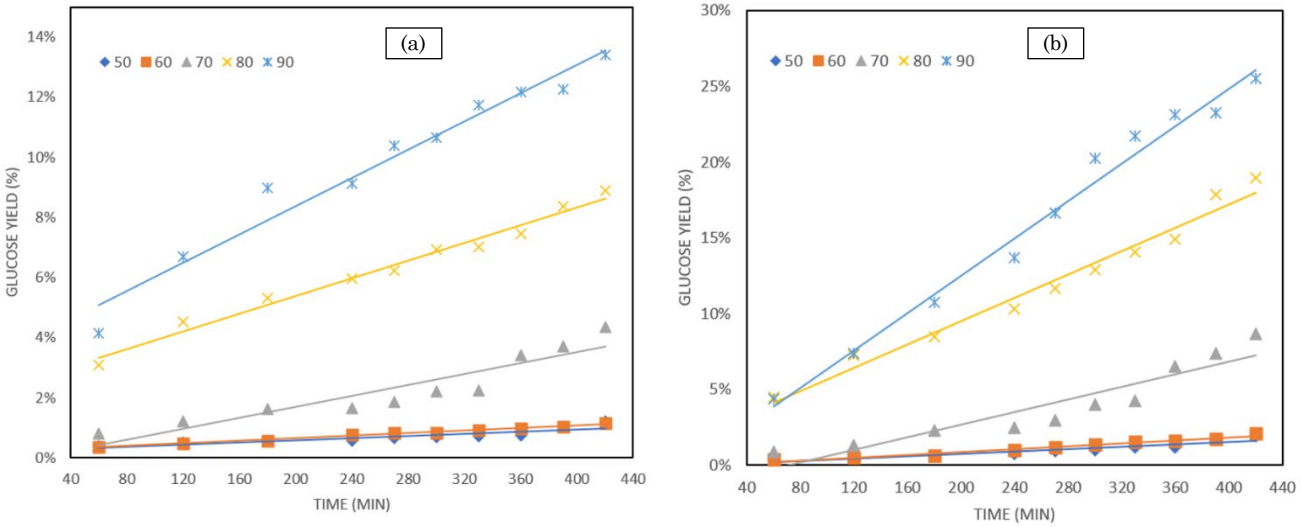


Figure 11. Glucose yield profiles as a function of reaction time at 50–90 °C using PDS catalyst with cellulose loadings of (a) 1 wt% and (b) 3 wt%.

Copyright © 2027, ISSN 1978-2993

acid catalysts (133–170 kJ/mol). This significant energy reduction demonstrates that the cooperative Brønsted acid-base relay provided by PDS successfully bypasses the high-energy pathways of random mineral acid hydrolysis under mild operational temperatures.

3.3. Cooperative Brønsted–Lewis Acid Synergy with Transition Metal Co-Catalysts

To explore the introduction of a dual Brønsted–Lewis acid synergistic environment, transition metal cations (Mn^{2+}, Cu^{2+}, Fe^{2+}, Zn^{2+}, and Ni^{2+}) were integrated at a fixed concentration of 0.006 M into the PDS catalytic phase. The temporal profiles of glucose generation across varied temperatures (50, 70, and 90 °C) are presented in Figure 13(a–c), and the extracted Arrhenius parameters are compiled in Table 10.

The pronounced divergence in apparent activation energies among the transition metal co-catalysts arises from differences in their aqueous ligand-exchange lability, Ligand-Field Stabilization Energy (LFSE), and chelation rigidity with cellulose hydroxyl groups: (1). Labile Lewis Acid Promoters (Fe^{2+}, Cu^{2+}, Mn^{2+}): High-spin Fe^{2+} (d^6), Jahn–Teller distorted Cu^{2+} (d^9), and high-spin Mn^{2+} (d^5) possess kinetically labile hydration shells that allow rapid, reversible coordination with the glycosidic and vicinal hydroxyl oxygens of cellulose. This dynamic coordination induces optimal electronic polarization ($C^{\delta+} - O^{\delta-}$) (Figure 14) and facilitates smooth cooperative proton transfer from PDS without trapping the substrate, maintaining low activation barriers (65.27–71.32 kJ.mol^{-1}) 2. Conformationally Locked Complexes (Ni^{2+} and Zn^{2+}): In contrast, Ni^{2+} (d^8) exhibits high octahedral LFSE, resulting in slow ligand-exchange kinetics, while Zn^{2+} (d^{10}) forms rigid, geometrically constrained chelate rings with the $C2/C3$ hydroxyl groups of glucopyranose units. This excessive complex rigidity sterically impedes the approach of the bulky piperazinium proton donor (NH^+) and restricts local chain mobility. Consequently, substantially higher thermal input $E_a =$

Table 9. Comparison of apparent activation energies for cellulose hydrolysis reported in the literature for various catalytic systems.

Catalytic system	Substrate	E_a [kJ/mol]	Operating cond.	Ref.
Dilute H_2SO_4	MCC	151	T: 150–200 °C	[13]
Fe-GO-SO_3H	Pure crystalline cellulose (DP 300)	12	T: 75 °C; t: 44 h; P: atm	[27]
Solid acids (CP-SO_3H, H_2SO_4)	Cellulose (Avicel; MCC); cellobiose; pretreated lignocellulose	CP-SO_3H (cellobiose): 78; CP-SO_3H (Avicel): 83 ; H_2SO_4 : 133–170	T: 75–180 °C; t: 1–48 h	[23]
PDS–metal system	Water hyacinth cellulose	65–104	T: 50–90 °C; t: 7 h	(this work)

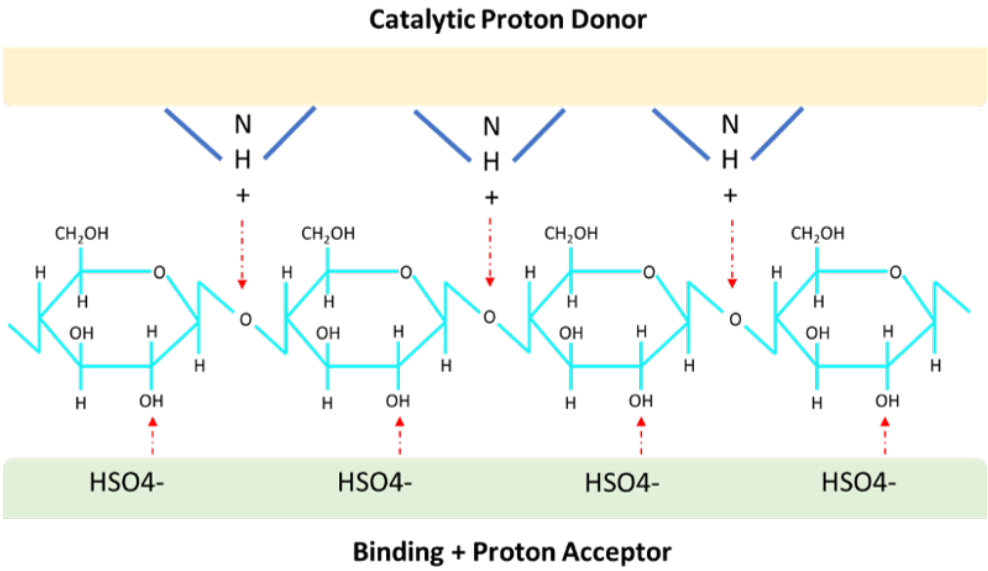


Figure 12. Proposed biomimetic catalytic mechanism for cellulose hydrolysis using PDS, illustrating proton-assisted cleavage of β-1,4-glycosidic bonds. The protonated piperazinium group (NH^+) acts as a proton donor, while the HSO_4^- species functions as a binding site and proton acceptor.

Copyright © 2027, ISSN 1978-2993

(93.84–103.72 kJ.mol^{-1}) is required to destabilize these overly stable metal–cellulose complexes prior to bond cleavage, manifesting as the observed Kinetic Compensation Effect.

4. Conclusions

This study demonstrates that hydrolysis of water hyacinth cellulose under mild conditions is strongly governed by the interplay between biomass structural accessibility and biomimetic

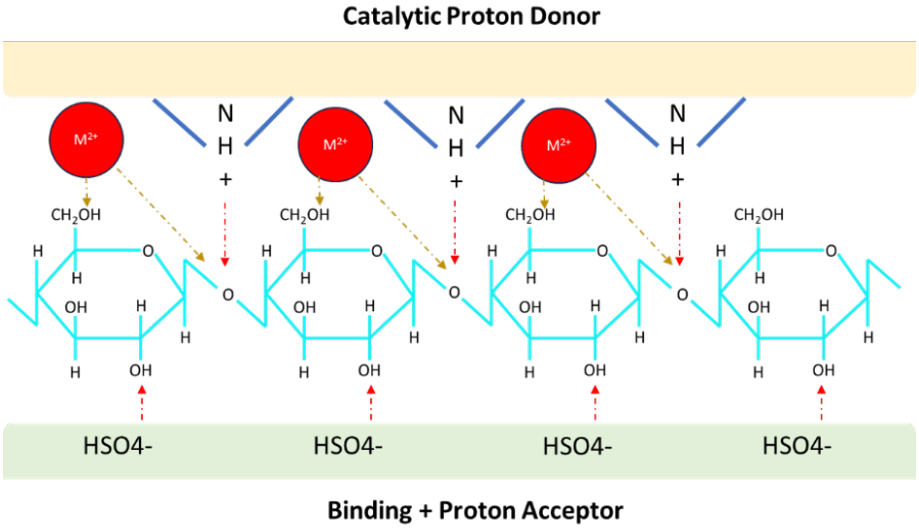


Figure 14. Proposed cooperative catalytic mechanism for cellulose hydrolysis involving Brønsted acid sites from PDS and Lewis acidic transition metal ions (M^{2+}). The metal ions coordinate with oxygen atoms in the cellulose structure, inducing polarization of the glycosidic bond ($O^{\delta-}$–$C^{\delta+}$) and weakening the C–O linkage, while proton transfer from PDS facilitates glycosidic bond cleavage.

Table 10. Activation energy (E_a) and pre-exponential factor (A) obtained from Arrhenius analysis for cellulose hydrolysis catalyzed by PDS alone and PDS combined with transition metal co-catalysts.

Catalyst	E_a [kJ/mol]	A
PDS	69.21	1.33×10^8
PDS+Mn	71.32	3.23×10^8
PDS+Cu	70.23	2.98×10^8
PDS+Fe	65.27	4.81×10^7
PDS+Zn	93.84	5.37×10^{11}
PDS+Ni	103.72	1.26×10^{13}

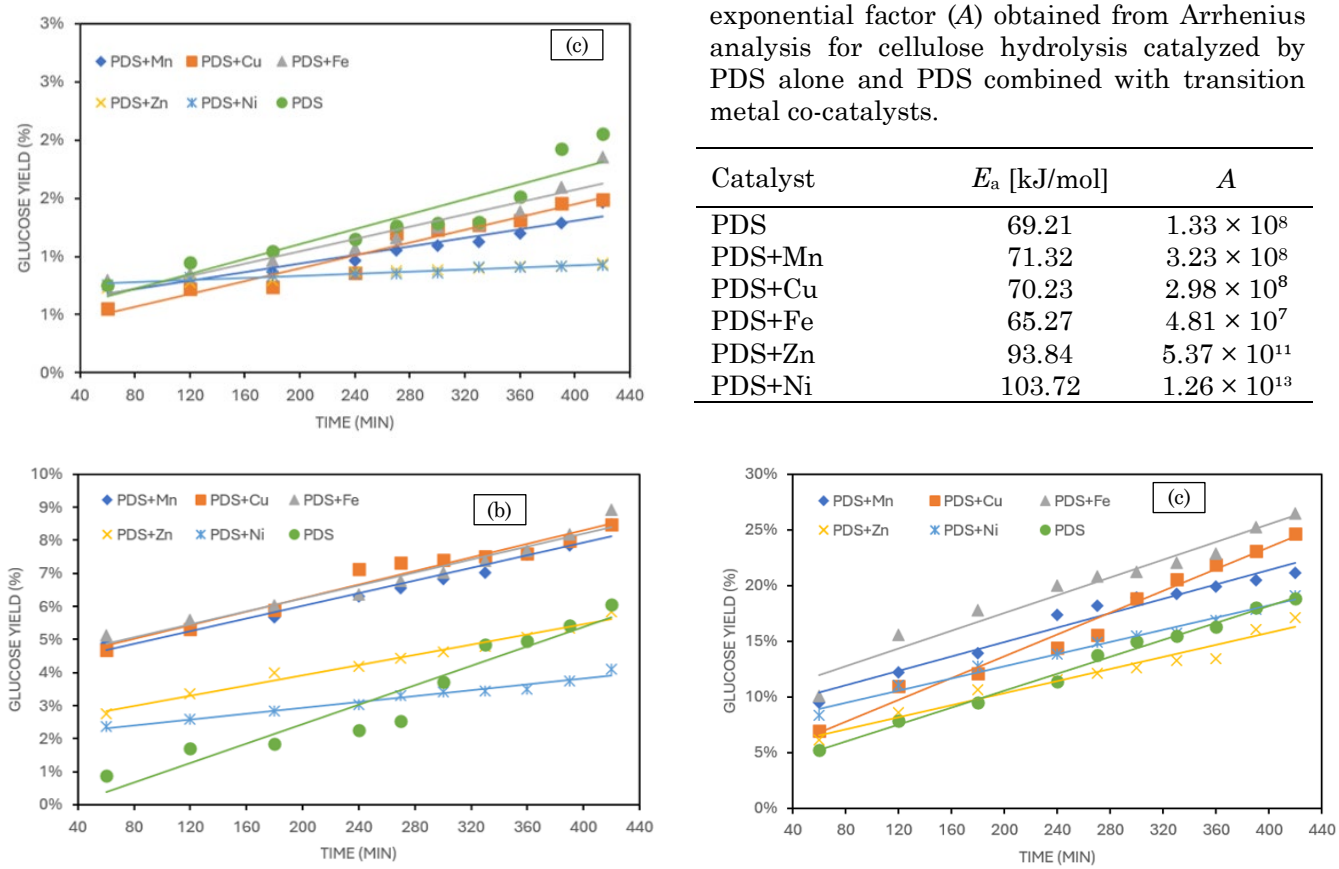


Figure 13. Glucose yield profiles as a function of reaction time for cellulose hydrolysis using PDS alone and PDS combined with transition metal co-catalysts: (a) 50 °C, (b) 70 °C, and (c) 90 °C.

Copyright © 2027, ISSN 1978-2993

catalytic activation. Sequential pretreatment effectively removed non-cellulosic components and altered the supramolecular organization of cellulose through disruption of hydrogen-bonding networks, fibril delamination, and partial reduction of crystallinity, resulting in a more accessible cellulose-rich structure with fibril diameters of 5–20 nm and a crystallinity index of 20.1%. Biomimetic hydrolysis using piperazinium dihydrogen sulfate (PDS) exhibited effective catalytic performance at 50–90 °C, yielding apparent rate constants of 0.0010–0.0346 $mmol.L^{-1}.min^{-1}$. Kinetic analysis revealed fractional reaction orders of 0.80 with respect to cellulose concentration and 0.75 with respect to proton concentration, indicating heterogeneous and structure-dependent hydrolysis behavior. The calculated activation energies (65–74 $kJ.mol^{-1}$) were substantially lower than those commonly reported for conventional mineral acid hydrolysis, demonstrating the effectiveness of the biomimetic proton relay mechanism in promoting glycosidic bond cleavage under mild conditions. The incorporation of transition metal co-catalysts, particularly Fe and Cu, further enhanced hydrolysis performance through cooperative Brønsted–Lewis acid interactions that facilitated bond polarization and catalytic activation. Overall, the results establish that cellulose depolymerization is controlled by an integrated structure–accessibility–catalysis relationship involving supramolecular organization, reactive-site accessibility, proton-transfer efficiency, and cooperative catalytic interactions, highlighting the potential of combining pretreatment engineering with biomimetic catalysis for sustainable lignocellulosic biomass valorization and renewable glucose production.

Acknowledgements

The authors gratefully acknowledge Institut Teknologi Bandung (ITB) for academic support. This research was supported and experimentally conducted at PT Aimtopindo Nuansa Kimia, whose facilities and technical assistance are greatly appreciated.

CRediT Author Statement

Authors Contributions: Mey Shelly Rikin: Writing – original draft, Methodology, Conceptualization, Data curation. Tri Partono Adhi: Writing – review & editing, Supervision, Project administration. Tjokorde Walmiki Samadhi: Writing – review, Supervision. Setyo Yanus Sasongko: Review, Methodology, Investigation, Supervision. All authors have read and agreed to the published version of the manuscript.

Declaration of Conflict of Interest

The authors declare that they have no known competing financial interests or personal relationships that could have appeared to influence the work reported in this paper. The research was conducted at PT. Aimtopindo Nuansa Kimia with academic support from Institut Teknologi Bandung.

Declaration of Generative AI Use

During the preparation of this work, the authors used AI to improve the language and readability of the manuscript. After using this tool, the authors reviewed, verified, and edited the content as needed. The authors take full responsibility for the content of the publication. The experimental design, data collection, data analysis, and scientific interpretation were carried out by the authors.

References

[1] Ragauskas, A.J., Williams, C.K., Davison, B.H., Britovsek, G., Cairney, J., Eckert, C.A., Frederick, W.J., Jr., Hallett, J.P., Leak, D.J., Liotta, C.L., Mielenz, J.R., Murphy, R., Templer, R., Tschaplinski, T. (2006). The path forward for biofuels and biomaterials. *Science*, 311(5760), 484–489. DOI: 10.1126/science.1114736.

[2] Rinaldi, R., Schüth, F. (2009). Design of solid catalysts for the conversion of biomass. *Energy & Environmental Science*, 2(6), 610–626. DOI: 10.1039/b902668a.

[3] Bozell, J.J., Petersen, G.R. (2010). Technology development for the production of biobased products from biorefinery carbohydrates—the US Department of Energy's "Top 10" revisited. *Green Chemistry*, 12(4), 539–554. DOI: 10.1039/b922014c.

[4] Malik, A. (2007). Environmental challenge vis a vis opportunity: The case of water hyacinth. *Environment International*, 33(1), 122–138. DOI: 10.1016/j.envint.2006.08.004.

[5] Gaurav, G.K., Mehmood, T., Cheng, L., Klemeš, J.J., Shrivastava, D.K. (2020). Water hyacinth as a biomass: A review. *Journal of Cleaner Production*, 277, 122214. DOI: 10.1016/j.jclepro.2020.122214.

[6] Sindhu, R., Binod, P., Pandey, A., Madhavan, A., Alphonsa, J.A., Vivek, N., Gnansounou, E., Castro, E., Faraco, V. (2017). Water hyacinth a potential source for value addition: An overview. *Bioresource Technology*, 230, 152–162. DOI: 10.1016/j.biortech.2017.01.035.

[7] Villamagna, A.M., Murphy, B.R. (2010). Ecological and socio-economic impacts of invasive water hyacinth (Eichhornia crassipes): A review. *Freshwater Biology*, 55(2), 282–298. DOI: 10.1111/j.1365-2427.2009.02294.x.

Copyright © 2027, ISSN 1978-2993

[8] Klemm, D., Heublein, B., Fink, H.-P., Bohn, A. (2005). Cellulose: Fascinating biopolymer and sustainable raw material. *Angewandte Chemie International Edition*, 44(22), 3358–3393. DOI: 10.1002/anie.200460587.

[9] Nishiyama, Y., Langan, P., Chanzy, H. (2002). Crystal structure and hydrogen-bonding system in cellulose Iß from synchrotron X-ray and neutron fiber diffraction. *Journal of the American Chemical Society*, 124(31), 9074–9082. DOI: 10.1021/ja0257319.

[10] Park, S., Baker, J.O., Himmel, M.E., Parilla, P.A., Johnson, D.K. (2010). Cellulose crystallinity index: Measurement techniques and their impact on interpreting cellulase performance. *Biotechnology for Biofuels*, 3, 10. DOI: 10.1186/1754-6834-3-10.

[11] Sun, Y., Cheng, J. (2002). Hydrolysis of lignocellulosic materials for ethanol production: A review. *Bioresource Technology*, 83(1), 1–11. DOI: 10.1016/S0960-8524(01)00212-7.

[12] Rinaldi, R., Schüth, F. (2009). Acid hydrolysis of cellulose as the entry point into biorefinery schemes. *ChemSusChem*, 2(12), 1096–1107. DOI: 10.1002/cssc.200900188.

[13] Girisuta, B., Janssen, L.P.B.M., Heeres, H.J. (2007). Kinetic study on the acid-catalyzed hydrolysis of cellulose to levulinic acid. *Industrial & Engineering Chemistry Research*, 46(6), 1696–1708. DOI: 10.1021/ie061186z.

[14] Weingarten, R., Cho, J., Xing, R., Conner, W.C., Jr., Huber, G.W. (2012). Kinetics and reaction engineering of levulinic acid production from aqueous glucose solutions. *ChemSusChem*, 5(7), 1280–1290. DOI: 10.1002/cssc.201100717.

[15] Zhang, Y.-H.P., Lynd, L.R. (2004). Toward an aggregated understanding of enzymatic hydrolysis of cellulose: Noncomplexed cellulase systems. *Biotechnology and Bioengineering*, 88(7), 797–824. DOI: 10.1002/bit.20282.

[16] Endo, T., Fujii, S., Aung, E.M., Kuroda, K., Tsukegi, T., Ninomiya, K., Takahashi, K. (2018). Cellulose structural change in various biomass species pretreated by ionic liquid at different biomass loadings. *BioResources*, 13(3), 6663–6677. DOI: 10.15376/biores.13.3.6663-6677.

[17] Mosier, N., Wyman, C., Dale, B., Elander, R., Lee, Y.Y., Holtzapple, M., Ladisch, M. (2005). Features of promising technologies for pretreatment of lignocellulosic biomass. *Bioresource Technology*, 96(6), 673–686. DOI: 10.1016/j.biortech.2004.06.025.

[18] Kumar, P., Barrett, D.M., Delwiche, M.J., Stroeve, P. (2009). Methods for pretreatment of lignocellulosic biomass for efficient hydrolysis and biofuel production. *Industrial & Engineering Chemistry Research*, 48(8), 3713–3729. DOI: 10.1021/ie801542g.

[19] Hubbell, C.A., Ragauskas, A.J. (2010). Effect of acid-chlorite delignification on cellulose degree of polymerization. *Bioresource Technology*, 101(19), 7410–7415. DOI: 10.1016/j.biortech.2010.04.029.

[20] Zhao, H., Kwak, J.H., Wang, Y., Franz, J.A., White, J.M., Holladay, J.E. (2006). Effects of crystallinity on dilute acid hydrolysis of cellulose by cellulose ball-milling study. *Energy & Fuels*, 20(2), 807–811. DOI: 10.1021/ef050319a.

[21] Breslow, R. (1982). Artificial enzymes. *Science*, 218(4572), 532–537. DOI: 10.1126/science.7123255.

[22] Vocadlo, D.J., Davies, G.J. (2008). Mechanistic insights into glycosidase chemistry. *Current Opinion in Chemical Biology*, 12(5), 539–555. DOI: 10.1016/j.cbpa.2008.05.010.

[23] Yang, G., Luo, X., Shuai, L. (2021). Bioinspired cellulase-mimetic solid acid catalysts for cellulose hydrolysis. *Frontiers in Bioengineering and Biotechnology*, 9, 770027. DOI: 10.3389/fbioe.2021.770027.

[24] Huang, Y.-B., Fu, Y. (2013). Hydrolysis of cellulose to glucose by solid acid catalysts. *Green Chemistry*, 15(5), 1095–1111. DOI: 10.1039/c3gc40136g.

[25] Rikin, M.S., Adhi, T.P., Soerawidjaja, T.H., Indarto, A., Sasongko, S.Y. (2025). Biomimetic hydrolysis of water hyacinth cellulose to glucose. *ASEAN Journal of Chemical Engineering*, 25(3), 493–508. DOI: 10.22146/ajche.19172.

[26] Segal, L., Creely, J.J., Martin, A.E., Jr., Conrad, C.M. (1959). An empirical method for estimating the degree of crystallinity of native cellulose using the X-ray diffractometer. *Textile Research Journal*, 29(10), 786–794. DOI: 10.1177/004051755902901003.

[27] Verma, D., Tiwari, R., Sinha, A.K. (2013). Depolymerization of cellulosic feedstocks using magnetically separable functionalized graphene oxide. *RSC Advances*, 3(32), 13265–13272. DOI: 10.1039/C3RA41025K.

[28] Kim, T.H., Yoo, C.G. Lamsal, B.P. (2013). Front-end recovery of protein from lignocellulosic biomass and its effects on chemical pretreatment and enzymatic saccharification. *Bioprocess. Biosyst. Eng*. 36(5), 687–694. DOI: 10.1007/s00449-013 0892-8

[29] dos Santos-Silva, A.C., Saraiva, B.R., Lazzari, A., dos Santos, H., de Oliveira, É.L., Sato, F., Meurer, E.C. Matumoto-Pintro, P.T. (2024). Optimization and characterization of protein extraction from asparagus leafy by-products. *Foods*, 13(6), 894. DOI: 10.3390/foods13060894

[30] Nynäs, A.L., Newson, W. R., Johansson, E. (2021). Protein fractionation of green leaves as an underutilized food source—protein yield and the effect of process parameters. *Foods*, 10(8), 2533. DOI: 10.3390/foods10112533

[31] Hubbel, C A., Ragauskas, A J. (2010). Effect of acid-chlorite delignification on cellulose degree of polymerization. *Biosour. Technol*. 101, 7410-7415. DOI: 10.1016/j.biortech.2010 .04.029.

Copyright © 2027, ISSN 1978-2993